

# An Incremental Sampling and Segmentation-Based Approach for Motion Planning Infeasibility

Antony Thomas and Fulvio Mastrogiovanni and Marco Baglietto

**Abstract**—We present a simple and easy-to-implement algorithm to detect plan infeasibility in kinematic motion planning. Our method involves approximating the robot’s configuration space to a discrete space, where each degree of freedom has a finite set of values. The obstacle region separates the free configuration space into different connected regions. For a path to exist between the start and goal configurations, they must lie in the same connected region of the free space. Thus, to ascertain plan infeasibility, we merely need to sample adequate points from the obstacle region that isolate start and goal. Accordingly, we progressively construct the configuration space by sampling from the discretized space and updating the bitmap cells representing obstacle regions. Subsequently, we partition this partially built configuration space to identify different connected components within it and assess the connectivity of the start and goal cells. We illustrate this methodology on five different scenarios with configuration spaces having up to 5 degree-of-freedom (DOF).

**Index Terms**—motion planning, motion planning infeasibility, configuration space obstacles

## I. INTRODUCTION

Motion planning is a fundamental problem in robotics, involving finding a path for a robot from its start configuration to a goal configuration without colliding with obstacles. A complete motion planner can either compute a collision-free path from the start to the goal or conclude that no such path exists. However, complete motion planning is challenging, and most approaches focus on finding a feasible plan with weaker notions of completeness. Resolution complete planners, typically those based on cell decomposition, offer completeness provided that the number of cells used to discretize the configuration space is sufficiently high [1]. Yet, in high-dimensional configuration spaces, such approaches tend to be computationally very expensive. Sampling-based motion planners [2], [3] are typically employed in such cases to find paths as quickly as possible. However, they are only probabilistically complete [4], meaning that if a plan exists, they will find it given enough time, but if no plan exists, they can run forever (or until a timeout). Therefore, a timeout is not a guarantee of infeasibility. In this work, we focus on the less examined path non-existence problem and present a simple algorithm that checks for motion planning infeasibility.

Motion infeasibility is a critical aspect of many robot planning methodologies. Task and motion planning [5]–[10] must consider the feasibility of motion plans to achieve

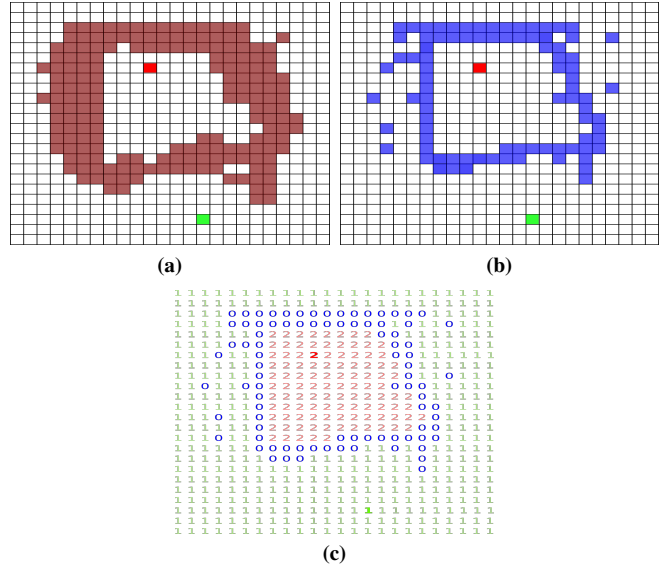


**Fig. 1:** (a) A representative discrete configuration space with the start and goal configuration cells colored in green and red, respectively. Other colored cells represent obstacle regions, while uncolored cells represent free space. (b) The sampled obstacle region is colored in blue. This partially constructed configuration space is sufficient to establish motion planning infeasibility since there exists no path from the start to the goal. (c) Segmented representation of the configuration space as shown in (b). There are two regions denoted by 1’s and 2’s, respectively, separated by the obstacle region indicated by 0’s. Since the start configuration belongs to region 1 and the goal configuration belongs to region 2, motion planning is infeasible.

the associated high-level tasks. When motion planning is deemed infeasible, alternative task plans must be generated. Similarly, feasibility checks are fundamental in manipulation tasks amidst clutter or rearrangement planning [11]–[14]. This often entails either displacing obstacles obstructing the task, usually identified through motion planning infeasibility, or positioning them at specific locations. The latter requires evaluating the feasibility of motion plans for different object placements.

The main contribution of this paper is a simple and easy-to-implement algorithm for proving the infeasibility of motion planning. We introduce a technique to demonstrate motion planning infeasibility by segmenting a discrete configuration space into distinct free regions isolated by the obstacle region. We note that such distinct free regions are referred to as connected components of the free space. Therefore, we use the terms *distinct free region*

\*Department of Informatics, Bioengineering, Robotics, and Systems Engineering, University of Genoa, Via All’Opera Pia 13, 16145 Genoa, Italy. antony.thomas@dibris.unige.it, fulvio.mastrogiovanni@unige.it, marco.baglietto@unige.it

and *connected component* interchangeably. If the start and goal configurations are partitioned into separate free regions, motion planning is deemed infeasible. However, computing a discrete configuration space is computationally expensive, especially for a robot with a high degree-of-freedom (DOF). To address this issue, we initially set the entire configuration space to free regions. Subsequently, we incrementally construct the configuration space by sampling and checking if the sampled configurations lie within the obstacle region. The key concept underpinning the incremental sampling is based on the principle that it is often unnecessary to sample the entire obstacle region. Instead, our objective is to draw a sufficient number of samples that establish the partition of the start and goal configurations into disconnected components of the configuration space. During each iteration, the partially constructed configuration space is segmented into distinct connected free regions as shown in Fig. 1. The segmented configuration space is then queried to determine whether the start and the goal configurations belong to the same connected free region. In Section IV, we elucidate this approach in detail and further discuss methods to speed up the construction of the configuration space.

## II. RELATED WORK

In this Section, we provide an overview of previous works related to motion planning infeasibility. These works are classified based on the different strategies employed to establish the non-existence of a feasible path.

*Approximate configuration space:* Zhang *et al.* [15] decompose the configuration space into cells, which are then queried to determine if they lie within the obstacle region. Subsequently, a graph is constructed where the nodes represent the cells and the edges represent adjacent cells. Using the cells that contain free regions, the problem of path non-existence is transformed into a graph search problem. Checking the occupancy of each cell is computationally challenging in higher dimensions. In contrast, our approach does not always require checking the occupancy of every cell. In a different approach presented in [16], obstacle regions are decomposed into collections of simplices called alpha shapes. These simplices are then utilized to address connectivity queries. However, methods for computing higher-dimensional alpha shapes are presently unknown. Points in the obstacle region are sampled to identify possible facets of a separating polytope in [17]. A separating polytope is a closed polytope that separates the start and goal into disconnected components of the free configuration space. However, the generation of these facets is computationally expensive, which can lead to scalability issues, especially in higher-dimensional configuration spaces. Varava *et al.* [18] construct an approximation of the obstacle region by decomposing it into a set of slices corresponding to subspaces of fixed obstacle orientations. They then compute the free space as the complement of this approximated obstacle region, which is subsequently used to synthesize a connectivity graph. A rigid body passing through a narrow gate is considered in [19]. The orientations of the rigid body are discretized,

and each orientation is individually checked for its ability to pass through the gate.

*Learning based:* Li *et al.* [20] combine supervised learning and sampling based planning to prove motion planning infeasibility. They achieve this by constructing an infeasibility proof, which involves learning a manifold contained within the obstacle region and querying whether it separates the start and the goal. However, they assume that it is always possible to sample on the manifold and compute the configuration space penetration depth of these samples. In [21], a representative roadmap is learned from available training problems, along with the probability of the edges being collision-free. Yet, the authors only prove the infeasibility in the roadmap and not the configuration space. Approaches in [22], [23] learn a classifier that guides the robot toward feasible motions. However, the classifier is used only as a heuristic to quickly estimate the feasibility of high-level actions rather than as an infeasibility proof.

*Feasibility through constraint modification:* The minimum constraint displacement (MCD) [24]–[26] and the minimum constraint removal (MCR) [27], [28] motion planning problems identify the minimum displacement of obstacles and the minimum number of obstacles to be removed, respectively, to guarantee a feasible motion plan. MCD class of problems does not inherently provide a means to prove infeasibility. If planning is infeasible, MCD computes the minimum displacement of obstacles required to ensure feasibility. The MCR class of problems is generally solved by partitioning the configuration space along the obstacle boundaries to obtain different connected regions that form a discrete graph. The MCR graph is then queried to determine the minimum number of obstacles to be removed to connect the start and the goal configuration. Implicitly, if the start and goal configurations are disconnected by obstacle regions, it implies that motion planning is infeasible. However, computing such partitions becomes intractable as the number of obstacles increases, especially in high-dimensional spaces.

For the majority of approaches categorized as *approximate configuration space* or *learning based*, the input typically comprises an approximate configuration space computed using techniques like cell decomposition or sampling-based methods [2], [3]. Notably, the overall computation time for determining infeasibility does not include the time taken for constructing the configuration space. In contrast to these approaches, our method involves the incremental construction of the configuration space, which constitutes the primary time-consuming task, as demonstrated in Section V. While MCD and MCR implicitly address infeasibility by identifying minimal obstacle displacements or sets that ensure plan feasibility, these problems remain NP-hard.

## III. PRELIMINARIES

We consider a robot  $\mathcal{R}$ , which operates in the workspace  $\mathcal{W} \subset \mathbb{R}^a$ , with  $a = 2$  or  $a = 3$ . An obstacle in  $\mathcal{W}$  will be denoted by  $\mathcal{O}$  and  $\mathcal{C}$  will be used to denote the configuration space (C-space in short) of the robot  $\mathcal{R}$ . A configuration  $q \in \mathcal{C}$  of  $\mathcal{R}$  completely specifies the volume

occupied by  $\mathcal{R}$ , and will be denoted by a list of  $n$  parameters  $q = (q^1, \dots, q^n)$ , where  $n$  is the dimension of  $\mathcal{C}$ . Therefore, given a configuration  $q$  of  $\mathcal{R}$ , the corresponding placement of  $\mathcal{R}$  in  $\mathcal{W}$  will be denoted by  $\mathcal{R}(q)$ . The obstacle region  $\mathcal{O} \subset \mathcal{W}$  maps into  $\mathcal{C}$  to the region C-obstacle  $= \{q \in \mathcal{C} \mid \mathcal{R}(q) \cap \mathcal{O} \neq \emptyset\}$ . Finally, C-free is the region in  $\mathcal{C}$  given by  $\mathcal{C} \setminus \text{C-obstacle}$ , that is, C-free  $= \{q \in \mathcal{C} \mid \mathcal{R}(q) \cap \mathcal{O} = \emptyset\}$ . The start and goal configurations will be denoted as  $q_s$  and  $q_g$ , respectively.

In this work, we limit the C-space to a discrete set, where each DOF is constrained to finite values. This discretized C-space will be called the C-space bitmap  $\mathcal{CB}$ . Thus, for a C-space of dimension  $n$  ( $n$  DOFs), we obtain an  $N^1 \times N^2 \times \dots \times N^n$  C-space bitmap  $\mathcal{CB}$ , where  $N^i$  is the resolution of the  $i$ -th DOF. Each cell of the  $n$ -dimensional  $\mathcal{CB}$  corresponds either to the C-free (denoted by 1) or the C-obstacle (denoted by 0)

As argued above, any configuration  $q \in \mathcal{C}$  of  $\mathcal{R}$  can be mapped to the subset of  $\mathcal{W}$  occupied by  $\mathcal{R}$ , that is,  $\mathcal{R}(q)$ . Therefore,  $\mathcal{CB}$  may be constructed by iterating over all possible  $n$ -tuples  $q = (q^1, \dots, q^n)$  belonging to the  $N^1 \times N^2 \times \dots \times N^n$  binary array such that  $\mathcal{CB}(q) = 1$  when  $\mathcal{R}(q)$  does not collide with any obstacle and  $\mathcal{CB}(q) = 0$ , when  $\mathcal{R}(q)$  collides with at least one obstacle. Checking for collision with obstacles for all configurations is computationally expensive, especially when dealing with higher resolutions and dimensions of configuration spaces. For the 4-DOF robot depicted in Fig. 3b, generating the complete  $\mathcal{CB}$  with a resolution of  $36 \times 36 \times 36 \times 36$  required approximately 58 minutes<sup>1</sup>. While methods for efficiently computing discrete C-space exist [30], [31], they tend to become prohibitively expensive as the dimension of the C-space increases.

#### IV. APPROACH

In a general perspective, our approach incrementally constructs the C-space bitmap  $\mathcal{CB}$ , by sampling configurations in C-obstacle. During each iteration, the updated  $\mathcal{CB}$  is segmented into different sets of adjacent *free* regions, akin to identifying distinct groups or regions of connected pixels in an image. We subsequently check whether the start ( $q_s$ ) and the goal ( $q_g$ ) reside in separate regions. Motion planning is infeasible if  $q_s$  and  $q_g$  are in different C-free regions. If the check fails, the iteration is repeated. The overall approach is summarized in Algorithm 1. Initially, all cells in the bitmap  $\mathcal{CB}$  are initialized to 1 (C-free). In each iteration, the subroutine `SampleCobstacle` is invoked (Algorithm 1, line 4), which samples at least  $ns$  configurations lying in C-obstacle. The cells of  $\mathcal{CB}$  corresponding to these C-obstacle samples are then set to zeros. The updated  $\mathcal{CB}$  is segmented to check whether  $q_s$  and  $q_g$  are in separate free regions (line 6). If they are in the same region, either a motion plan exists, or  $\mathcal{CB}$  needs to be updated with more samples from the C-obstacle to prove infeasibility.

<sup>1</sup>To check for collisions with obstacles, both the robot and obstacle polygons are subdivided into triangles, and a triangle intersection algorithm [29] is used. Computation performed on an Intel® Core i7-10510U CPU@1.80GHz×8 with 16GB RAM under Ubuntu 18.04 LTS.

---

#### Algorithm 1 Motion Planning Infeasibility Detection

---

**Input:**  $\mathcal{R}, q_s, q_g, \text{Obstacles}, n, ns$   
 $\triangleright ns$  denotes the minimum number of C-obstacle configurations sampled in each iteration.  
1:  $\mathcal{CB} \leftarrow \text{true}(N^1, \dots, N^n)$   
2:  $SS[0, \dots, sc - 1]$  be an array with  $sc = N^1 * N^2 * \dots * N^n$ , the size of  $\mathcal{CB}$   
3: **while true do**  
4:    $\mathcal{CB} \leftarrow \text{SampleCobstacle}$   
5:    $L \leftarrow \text{SegmentCB}$   
6:   **if** `SegmentCheck`( $L, q_s, q_g$ ) **then**  
7:     **return** No Motion Plan

---



---

#### Algorithm 2 SampleCobstacle

---

**Input:**  $\mathcal{R}, \text{Obstacles}, SS, ns, d$   
1: **for**  $i = 1, 2, \dots, ns$  **do**  
2:   **while true do**  
3:      $idx \leftarrow \text{RandomSample}(SS)$   
4:      $SS(idx) \leftarrow \emptyset$   
5:      $q \leftarrow \text{GetConfig}$   
6:      $cc, p \leftarrow \text{CollisionCheck}(\mathcal{R}(q), \text{Obstacles})$   
7:     **if**  $cc$  **then**  
8:        $\mathcal{CB}(idx) \leftarrow \text{false}$   
9:        $\mathcal{CB} \leftarrow \text{SpeedUp}(q, p)$   
10:       **for**  $d$  neighbors of  $q$  **do**  
11:           $\triangleright d$  neighbors of  $q$  randomly selected.  
12:           $SS(\cdot) \leftarrow \emptyset$   
13:           $q \leftarrow \text{GetConfig}$   
14:           $cc, p \leftarrow \text{CollisionCheck}(\mathcal{R}(q), \text{Obstacles})$   
15:          **if**  $cc$  **then**  
16:            $\mathcal{CB}(\cdot) \leftarrow \text{false}$   
17:            $\mathcal{CB} \leftarrow \text{SpeedUp}(q, p)$   
18:       **else**  
19:          **continue**  
20:   **return**  $\mathcal{CB}, SS$

---

##### A. Sampling C-obstacle

Since we initialize all cells in  $\mathcal{CB}$  as C-free, we need to sample configurations in C-obstacle to progressively build  $\mathcal{CB}$ . We maintain a set  $SS$  (Algorithm 1, line 2) that stores the linear indices corresponding to the multidimensional subscripts of  $\mathcal{CB}$ . Each multidimensional subscript in  $\mathcal{CB}$  corresponds to a configuration in the C-space. Algorithm 2 samples without replacement from the set  $SS$  until at least  $ns$  configurations in C-obstacle are selected. Each sampled configuration  $q$  is checked for collision (Algorithm 2, line 6). If  $\mathcal{R}(q) \in \text{C-obstacle}$ , the subroutine `CollisionCheck` returns a true value ( $cc$ ), and the corresponding  $\mathcal{CB}$  cell is updated to 0 (Algorithm 2, line 8), indicating that the cell belongs to C-obstacle. The fundamental concept behind incrementally sampling from the C-space is based on the fact that we do not always need to sample the whole C-obstacle space but only draw enough samples from C-obstacle to

separate the start and goal configurations into disconnected components in the C-space.

A significant computational bottleneck in Algorithm 2 is the `CollisionCheck` subroutine, which, for each sampled configuration  $q$ , checks for collisions between  $\mathcal{R}(q)$  and all obstacles in the environment. To optimize this process, we employ a simple heuristic that allows for avoiding unnecessary collision checks for certain configurations  $q$ . We will clarify this with an illustrative example. Let us consider an articulated robot with  $n$  links. Suppose that the  $j$ -th link, for a sampled configuration  $q = (q^1, \dots, q^j, \dots, q^n)$ , collides with an obstacle. In such a case, it is readily observed that

$$\forall q \mid q = (q^1, \dots, q^j, *) \implies \mathcal{R}(q) \in \text{C-obstacle} \quad (1)$$

where  $*$  denotes the fact that the components  $(q^{j+1}, \dots, q^n)$  may assume any admissible values. In other words, for all configurations where the components from the first link to the  $j$ -th link are fixed (values corresponding to those that resulted in collision with the obstacle), any combinations of the  $(j+1)$ -th to  $n$ -th links will still collide with that obstacle. Thus, without querying the `CollisionCheck` subroutine, all the cells in  $\mathcal{CB}$  corresponding to such configurations may be updated. A similar strategy may be employed in the case of C-obstacle formed due to self-collision. If the  $i$ -th link and the  $j$ -th link collide, it is verified that

$$\forall q \mid q = (*, q^i, \dots, q^j, *) \implies \mathcal{R}(q) \in \text{C-obstacle} \quad (2)$$

where  $*$  denotes the fact that the components  $(q^1, \dots, q^{i-1})$ ,  $(q^{j+1}, \dots, q^n)$  may assume any admissible values.

The process described above is achieved by calling the `SpeedUp` subroutine (line 9), which takes the colliding link(s)  $p$  as input. Similarly, in the case of a mobile robot that can rotate and translate, if a sampled configuration  $q$  is such that  $\mathcal{R}(q) \in \text{C-obstacle}$ , and the rotation axis of the robot intersects with an obstacle, then all rotations of the robot at that location will result in a collision. Hence, the configurations corresponding to all possible rotations with the fixed robot location are readily classified as C-obstacle, eliminating the need to query the `CollisionCheck` subroutine.

Finally, we also check for nearby configurations in collision (lines 10-16). Here we leverage the fact that if a specific configuration is in collision, nearby configurations are likely to be in collision as well. For this purpose, we randomly select  $d$  neighbors of a sampled  $q \in \text{C-obstacle}$ . The total number of neighbors of  $q$  depends on the C-space dimension, and further discussion on this is provided in Section V. The subroutine `SampleCobstacle` returns the updated  $\mathcal{CB}$  which is then segmented into different connected components for checking motion planning infeasibility.

### B. $\mathcal{CB}$ Segmentation

Since we only consider kinematic motion planning, infeasibility arises from the obstacle region (C-obstacle) in the C-space. Therefore, a motion plan exists only if  $q_s$  and  $q_g$  are not separated by C-obstacle; in other words, they must reside in the same connected component of the C-free space. Conversely, motion planning is infeasible if  $q_s$  and  $q_g$  are

separated by C-obstacle into different connected components. Formally, an infeasibility proof is a closed manifold that entirely resides within C-obstacle and separates the start and the goal [20].

The `SegmentCB` subroutine (Algorithm 1, line 5) segments  $\mathcal{CB}$  into different connected C-free regions separated by C-obstacle. The `SegmentCheck` function (Algorithm 1, line 6) verifies whether the start and goal components are separated by C-obstacle. If they are divided into different C-free regions, then motion planning is infeasible.

To achieve segmentation, we utilize an off-the-shelf segmentation function that assigns labels to different connected C-free regions. If  $q_s$  and  $q_g$  receive the same label, it indicates that they belong to the same connected C-free region, and thus, a motion plan exists. However, if they are assigned different labels, it does not immediately imply the absence of a motion plan. This is because, in scenarios involving motion planning for manipulators, it is essential to consider that orientations are defined modulo  $2\pi$  (assuming there are no joint limits). Therefore, when verifying the disconnection between  $q_s$  and  $q_g$ , the `SegmentCheck` subroutine takes into account the fact that orientation wraps around at  $2\pi$ .

### C. Analysis of $\mathcal{CB}$ Resolution

The C-obstacle region divides the C-free of the C-space  $\mathcal{C}$  into different connected free regions. For a given  $\mathcal{R}$  and  $\mathcal{W}$ , let us denote the different free regions by  $C^1, \dots, C^m$ , whose union results in C-free, denoted as  $\text{C-free} = \bigcup C^j$ . Let the connected free regions in  $\mathcal{CB}$  be denoted by  $D^1, \dots, D^l$ . We say that  $\mathcal{CB}$  is *equivalent* to  $\mathcal{C}$  if

- 1)  $l = m$
- 2)  $D^1 \subset C^1, \dots, D^l \subset C^m$
- 3)  $q_s \in \bigcup D^j$
- 4)  $q_g \in \bigcup D^j$

**Proposition 1.** Let  $\mathcal{C}$  be the configuration space corresponding to  $\mathcal{R}$  in  $\mathcal{W}$ . Given  $q_s$  and  $q_g$  configurations in  $\mathcal{C}$  such that motion planning is infeasible, then for any discretized configuration space  $\mathcal{CB}$  that is equivalent to  $\mathcal{C}$ , motion planning remains infeasible for  $q_s$  and  $q_g$  configurations in  $\mathcal{CB}$ .

**Proof.** Let  $q_s \in C^i$  and  $q_g \in C^j$ , so that motion planning is infeasible. From the definition of an equivalent  $\mathcal{CB}$ , we have  $D^k \subset C^k, \forall k \leq l, q_s \in \bigcup D^k$ , and  $q_g \in \bigcup D^k$ . Therefore, it follows that  $q_s \in D^i$  and  $q_g \in D^j$ . Thus, no motion plan exists.  $\square$

This concept is visualized in Fig. 2. A 2-link robot in its workspace, is shown in Fig. 2a, where the start and goal states are represented by green and red, respectively. Various obstacles are shown in different colors. The corresponding C-space  $\mathcal{C}$  is displayed in Fig. 2b, which illustrates how obstacles in the workspace translate into the C-space. The C-space is discretized at 0.1 degree for each DOF, resulting in a  $3600 \times 3600$  bitmap. The topology of the C-space is actually a torus, meaning the top and bottom edges are connected to each other, and the left and right edges are connected to each

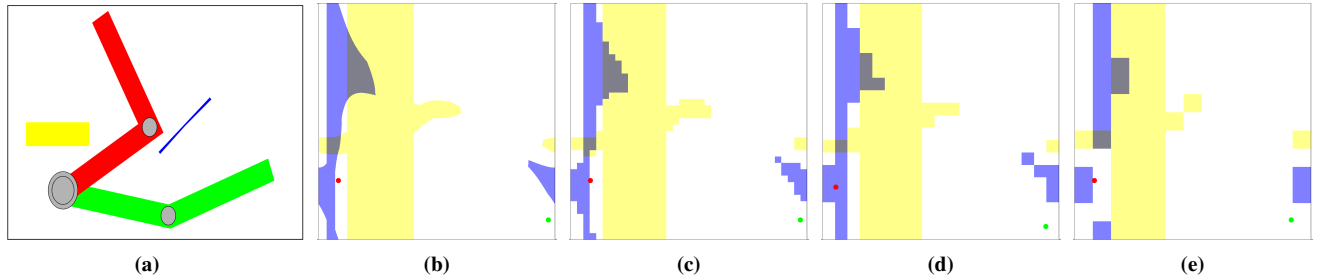


**Fig. 2:** (a) 2-link robot in its workspace. (b) The configuration space  $\mathcal{C}$ . The start and goal configurations are shown as green and red dots, respectively. The different colors represent the correspondence between obstacles in the workspace and obstacles in the C-space. (c) C-space with  $36 \times 36$  resolution. (d) C-space with  $18 \times 18$  resolution. (e) C-space with  $12 \times 12$  resolution.

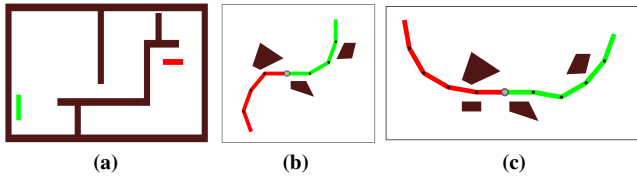


**Fig. 3:** Different types of robots employed for the 2D experiments. The start configuration of the robot is indicated by green color and the end configuration is denoted by red color. (a)  $S_1$ : 3-DOF rectangular robot scene. (b)  $S_2$ : 4-DOF articulated robot scene. (c)  $S_3$ : A 5-DOF articulated robot scene.

other. Thus, there are three connected components, and no feasible motion plan exists since  $q_s$  and  $q_g$  are not in the same connected component. Fig. 2c shows a  $\mathcal{CB}$  with resolution  $36 \times 36$  which is equivalent to  $\mathcal{C}$ . It can be easily verified that there is no collision-free path between  $q_s$  and  $q_g$  since they are in different connected components. A  $\mathcal{CB}$  of resolution  $18 \times 18$  is visualized in Fig. 2d. Although it has the same number of connected components, condition 4 is violated ( $q_g$  is incorrectly identified as inside a C-obstacle), and  $\mathcal{CB}$  is not equivalent to  $\mathcal{C}$ . Fig. 2e shows a  $\mathcal{CB}$  with a much lower resolution of  $12 \times 12$ . With only a single connected component, it is clearly not equivalent to  $\mathcal{C}$ , and wrongly certifies that motion planning is feasible.

#### D. Resolution-completeness

The discussed approach is resolution complete. Given sufficient resolution  $N^1 \times N^2 \times \dots \times N^n$  of the C-space, our algorithm either reports motion planning infeasibility or conclude that motion planning is feasible.

It is important to note that if a motion plan exists, Algorithm 1 continues to run until all cells in the  $\mathcal{CB}$  bitmap are sampled. Only then can it conclude that a motion plan exists after segmenting the  $\mathcal{CB}$  and verifying that start and goal are in the same connected region. Our approach is primarily designed for determining plan infeasibility, and the verification of plan feasibility should be performed using suitable sampling-based planners.

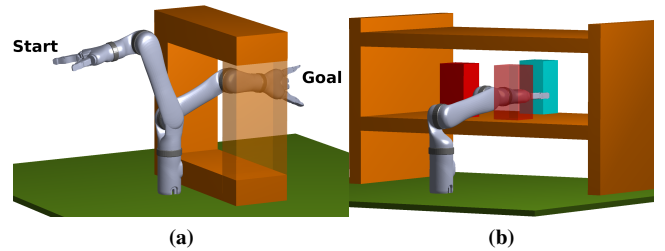


**Fig. 4:** Experiment scenes involving the 4-DOF Kinova arm: (a)  $S_4$ : The Kinova arm attempting to reach inside the frame. (b)  $S_5$ : The robot arm trying to grasp the cyan block from a position outside the shelf. The red blocks segment the start and goal configurations into different connected components, preventing any path.

## V. EXPERIMENTS

We conducted experiments on five different motion planning problems in both 2D and 3D workspaces. The 3D workspace scenarios, inspired by [20], are conducted using the 4-DOF Kinova MICO arm. The scenarios are as follows: ( $S_1$ ) A scenario involving a 2D robot capable of translation and rotation (see Fig. 3a), ( $S_2$ ) A scenario with a 4-DOF articulated robot, as depicted in Fig. 3b, ( $S_3$ ) A scenario involving a 5-DOF articulated robot aiming to reach a goal configuration (Fig. 3c), ( $S_4$ ) A scenario where the Kinova arm is trying to reach inside a frame (see Fig. 4a), and ( $S_5$ ) A scenario with the Kinova arm attempting to grasp the cyan block from a position outside the shelf, as shown in Fig. 4b.

The C-space resolution and the parameters  $ns$  and  $d$  for the `SampleCobstacle` subroutine are determined through empirical tuning. Unless otherwise mentioned, for the 2D scenarios, we empirically set  $ns = 10$ ,  $d = 5$  and for the 3D scenarios we empirically set  $ns = 100$ ,  $d = 5$ . Collision detection for the Kinova MICO arm is conducted using the `checkCollision`<sup>2</sup> feature of the MATLAB Robotics and Autonomous Systems toolbox. However, for the 2D scenarios, both the robot and obstacle polygons are subdivided into triangles, and a triangle intersection algorithm [29] is

<sup>2</sup>Web: <https://it.mathworks.com/help/robotics/ref/rigidbodytree.checkcollision.html>

Scenarios	Resolution	$n_s$	$d$	Iterations	Segmentation time (s)	Total time (s)
$S_1$ (Fig. 3a)	34×20×36	1000	10	1.60±0.56	$3.00 \times 10^{-3} \pm 3.00 \times 10^{-3}$	1.90±0.66
	67×39×72			2.50±1.50	0.01±0.00	2.93±1.68
	331×191×180			29.07±22.63	0.70±0.02	63.71±49.04
$S_2$ (Fig. 3b)	36×36×36×36	10	5	1.10±0.31	0.31±0.04	0.48±0.16
	48×48×48×48			1.03±0.18	1.04±0.11	1.42±0.29
	72×72×72×72			1.20±0.46	6.32±0.61	9.12±3.11
$S_3$ (Fig. 3c)	36×36×36×36×36	100	5	1.00±0.00	36.00±1.63	40.78±1.93
	48×48×48×48×48			1.00±0.00	170.78±11.78	189.36±14.09
	72×72×72×72×72			-	-	-
$S_4$ (Fig. 4a)	36×36×36×36	100	5	4.30±1.36	0.39±0.02	35.70±11.07
	48×48×48×48			7.00±2.44	1.18±0.04	76.28±25.92
	72×72×72×72			8.53±2.06	6.22±0.18	295.31±67.28
$S_5$ (Fig. 4b)	36×36×36×36	100	5	4.80±1.99	0.43±0.02	46.05±19.34
	48×48×48×48			8.33±3.83	1.30±0.05	98.69±45.01
	72×72×72×72			13.26±5.31	7.17±0.12	445.76±173.21

**TABLE I:** Motion planning infeasibility results. Resolution represents the finite values attainable for each DOF, that is, the resolution of  $\mathcal{CB}$ . Iterations denotes the average number of iterations to determine motion planning infeasibility. Total time is the overall time taken to report plan infeasibility. '-' indicates that the algorithm did not report any solution within 2000 seconds.

utilized for collision detection. The segmentation of  $\mathcal{CB}$  in the `SegmentCB` subroutine is accomplished by utilizing the MATLAB function `bwlabeln`<sup>3</sup>. This function returns a labeled matrix, assigning labels to different connected components. When checking for connectivity, the algorithm considers the full neighborhood in each dimension—the level of connectivity in each dimension is passed as an input to the `bwlabeln` function. For instance, in a 2-dimensional C-space, there can be a maximum of 8 neighbors, while in a 3-dimensional C-space, there can be up to 26 neighbors, and up to 80 in 4-dimensional spaces, and so on. Thus, for each sampled  $q \in \mathcal{C}$ -obstacle, the `SampleCobstacle` subroutine randomly selects  $d$  neighbors from  $q$ 's full neighborhood. The performance is evaluated on an Intel® Core i7-10510U CPU@1.80GHz×8 with 16GB RAM under Ubuntu 18.04 LTS.

Each experimental scenario corresponds to the non-existence of a path between the start and the goal configurations. To establish the ground truth for plan infeasibility, for the Kinova arm scenarios, we run RRT-Connect [3] continuously for more than 30 minutes, and for the other three scenarios, we run PRM [2] for more than 30 minutes. For each experiment, we conduct 30 trials and record the following metrics.

- The average number of iterations and the standard deviation needed to determine motion planning infeasibility. Note that a single iteration of Algorithm 1 involves sampling at least  $n_s$  configurations in C-obstacle.
- The average running time and standard deviation for the  $\mathcal{CB}$  segmentation subroutine, `SegmentCB`.
- The mean total run-time and standard deviation for Algorithm 1 to determine plan infeasibility.

Table I reports the above metrics, along with the parameters  $n_s$  (minimum number of samples generated by the subroutine `SampleCobstacle`) and  $d$  (number of nearby

configurations examined for collision). While the smallest resolution of  $\mathcal{CB}$  reported in Table I for each experiment is equivalent to their respective C-space and successfully identifies plan infeasibility, we also assess the computation times for higher resolutions of the C-space bitmap.

*3-DOF scenario:* Infeasibility is detected within a few seconds for the two lower resolutions. The higher resolution  $\mathcal{CB}$  reports a runtime of about a minute due to the corresponding increase in the number of C-obstacle samples necessary to segment  $q_s$  and  $q_g$  into different connected regions. However, it is worth noting that the segmentation of the  $\mathcal{CB}$  into connected C-free components takes only a fraction of a second for all three resolutions reported. We can conclude that the approach is applicable to 3-DOF robots.

*4-DOF experiments:* The scenarios presented in Fig. 3b and Fig. 4 involve a four-dimensional C-space. As observed in Table I, the average segmentation times for the three experiments are similar. However, the difference in the overall running time of the approach is primarily attributed to the distribution of obstacle regions within the workspace. In Fig.3b, due to the sparse obstacle distribution, for each sampled  $q \in \mathcal{C}$ -obstacle, using the `SpeedUp` subroutine and checking the  $d$  neighbors, configurations in C-obstacle that contribute to infeasibility are quickly identified. For the scenarios in Fig. 4a and Fig. 4b, dense obstacle regions necessitate a greater number of samples to identify C-obstacle configurations that contribute to infeasibility. This is evident in the scenario in Fig. 4b, where it is the two red blocks that prevent the arm from reaching the position shown in the figure. Due to the random sampling, currently, a large number of samples (those of the shelf) that are not related to infeasibility are also processed. Furthermore, the `CollisionCheck` subroutine for the 2D scenario using triangle intersection is much faster than the `checkCollision` function used for the scenarios in Fig. 4a-4b. We can conclude that our approach is well-suited for 4-DOF robots.

<sup>3</sup>Web: <https://it.mathworks.com/help/images/ref/bwlabeln.html>

*5-DOF scenario:* The approach demonstrates effective scalability to a 5-dimensional C-space, successfully detecting plan infeasibility within 40 seconds for lower resolution C-space. However, it's noteworthy that in this case, the segmentation process is the most time-consuming. When the bitmap size is increased to 48 in each dimension, the overall running time increases by approximately 5 times, primarily due to the segmentation of  $\mathcal{CB}$ . For the higher resolution of 72 in each dimension, the `SegmentCB` subroutine did not complete within 2000 seconds. In attempting to accommodate the maximum connectivity within a 5-dimensional bitmap (each  $q$  connected to  $3^5 - 1 = 242$  neighbors in this case), the `bwlabeln` function was unable to segment the large binary  $\mathcal{CB}$  within the specified cutoff time.

## VI. DISCUSSION

Plan infeasibility arises when  $q_s$  and  $q_g$  are situated in different connected components of the C-free space. Since we initialize all cells of the  $\mathcal{CB}$  as free regions, these cells need to be verified for occupancy. If the maximum resolution in any dimension of the C-space is  $N$ , in the worst case,  $N^a$  cells have to be verified, where  $a \leq 5$ . Thus, the overall computational complexity is  $O(N^a)$ . However, as elucidated in Section IV, the presented approach is based on the principle that it is not necessary to sample all points in the C-obstacle, but only those necessary to prove infeasibility. Consequently, for configuration spaces with up to 5 dimensions, the approach delivers reasonable performance in terms of computation time, detecting infeasibility in less than a minute.

The primary computational challenge lies in determining whether a sampled configuration falls within the C-free or C-obstacle region by running the `CollisionCheck` subroutine. Currently, we do not employ any specific sampling technique and instead sample randomly without replacement from the  $\mathcal{CB}$  bitmap to check for occupancy. An engineered approach to sampling from the obstacle region can significantly accelerate this bottleneck, as it allows to avoid sampling numerous C-free elements, thereby reducing the unnecessary execution of the `CollisionCheck` subroutine. Furthermore, parallelizing the sampling procedure can reduce the total runtime in all experiments.

Fig. 5a illustrates a modified version of the scenario depicted in Fig. 4a, where the obstacle region at the top and bottom is expanded, and the width of the vertical column is decreased, thereby increasing the overall obstacle region in the workspace. Despite the increased obstacle region, the overall runtime remained unaffected ( $37.99 \pm 11.94$  seconds and  $73.92 \pm 24.48$  seconds for resolutions of  $36 \times 36 \times 36 \times 36$  and  $48 \times 48 \times 48 \times 48$ , respectively). However, in general, an increase in the C-obstacle region is expected to result in longer runtimes.

For higher-dimensional C-spaces, the segmentation function currently employed becomes intractable while accommodating the maximum connectivity. Exploring alternative segmentation approaches, such as segmenting parts of the C-space and then combining them, presents potential avenues

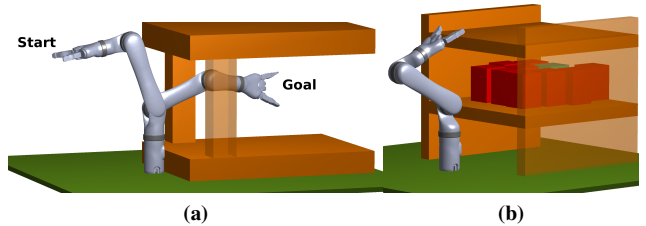


**Fig. 5:** (a) A Kinova arm attempts to reach inside the frame. Compared to the scenario in Fig. 4a, the top and bottom of the frame are expanded, and the vertical columns are compressed. The columns are made thinner so that the corresponding C-obstacle region contributing to infeasibility is also reduced in width. (b) The robot attempting to pick the cyan block from inside the shelf.

for future research to scale the proposed approach to higher-dimensional C-space.

The resolution of  $\mathcal{CB}$  must be such that it is equivalent to the C-space of the robot (see Section IV-C). Thus, selecting an adequate resolution for  $\mathcal{CB}$  is crucial since a lower resolution can lead to incorrect results (Fig. 2). In general, an adequate resolution is scenario dependent and primarily relies on factors such as the size of the robot and obstacles, as well as the distribution of obstacles in the workspace. For manipulators, a resolution of 36 or 48 (or higher) in each dimension produces an equivalent  $\mathcal{CB}$  in all the experiments considered in this work.

The values for  $ns$  and  $d$  are empirically determined. For the manipulator scenarios employing the 4-DOF robot, increasing the neighbors to  $d = 10$  did not result in any significant difference in the overall runtime. However, lower values of  $d < 5$ , or not checking for neighbor collision ( $d = 0$ ), resulted in higher running times due to the increased number of configurations that need to be sampled and checked for occupancy. Lower or higher values of  $ns$  did not significantly affect the runtimes. This arises from a trade-off between the segmentation time and the duration required for the `SampleCobstacle` subroutine. When  $ns$  is increased, the iterations decrease, thus reducing the segmentation time. However, more values need to be sampled and checked for collision. When  $ns$  is decreased, more iterations are required, thereby increasing the part of the overall runtime related to segmentation. For the 5-DOF robot, a lower value of  $ns$  implies more iterations and therefore results in a higher total runtime due to the increased time required for the segmentation of  $\mathcal{CB}$ .

There exist a class of infeasibility problems in which goal states may lie within the C-obstacle. For example, in the scenario depicted in Fig. 5b, the cyan block cannot be picked since other red blocks hinder the grasp. For such scenarios, it is common practice to sample gripper poses and derive corresponding grasp configurations via inverse kinematics when all other objects are absent from the workspace [6]. Then, it is checked whether all the grasp configurations fall within the C-obstacle region.

## VII. CONCLUSION

In this paper, we introduce a simple algorithm that is easy to implement for checking motion planning infeasibility. Our approach relies on the approximation of the C-space using a discretized bitmap. Initially, all cells of this bitmap are designated as C-free. Subsequently, our algorithm incrementally builds the bitmap by randomly sampling from the C-space and verifying the occupancy of each sampled cell. The constructed bitmap is then segmented into different connected components, which are separated by C-obstacles. Afterward, we query the connectivity of the start and goal cells. Through the incremental construction of the C-space, we only need to draw a sufficient number of samples to establish the partition between the start and goal configurations. The approach is validated through experiments involving robots with up to 5-DOF. We also discuss additional enhancements aimed at significantly accelerating the discussed algorithm, which are promising directions for future work.

## REFERENCES

- [1] L. Zhang, Y. J. Kim, and D. Manocha, "A hybrid approach for complete motion planning," in *2007 IEEE/RSJ International Conference on Intelligent Robots and Systems*, pp. 7–14, IEEE, 2007.
- [2] L. E. Kavraki, P. Svestka, J.-C. Latombe, and M. H. Overmars, "Probabilistic roadmaps for path planning in high-dimensional configuration spaces," *IEEE Transactions on Robotics and Automation*, vol. 12, no. 4, pp. 566–580, 1996.
- [3] J. J. Kuffner and S. M. LaValle, "Rrt-connect: An efficient approach to single-query path planning," in *Robotics and Automation, 2000. Proceedings. ICRA'00. IEEE International Conference on*, vol. 2, pp. 995–1001, IEEE, 2000.
- [4] S. Karaman and E. Frazzoli, "Sampling-based algorithms for optimal motion planning," *The International Journal of Robotics Research*, vol. 30, no. 7, pp. 846–894, 2011.
- [5] L. P. Kaelbling and T. Lozano-Pérez, "Integrated task and motion planning in belief space," *The International Journal of Robotics Research*, vol. 32, no. 9–10, pp. 1194–1227, 2013.
- [6] S. Srivastava, E. Fang, L. Riano, R. Chitnis, S. Russell, and P. Abbeel, "Combined task and motion planning through an extensible planner-independent interface layer," in *Robotics and Automation (ICRA), IEEE International Conference on*, pp. 639–646, IEEE, 2014.
- [7] F. Lagriffoul, D. Dimitrov, J. Bidot, A. Saffiotti, and L. Karlsson, "Efficiently combining task and motion planning using geometric constraints," *The International Journal of Robotics Research*, vol. 33, no. 14, pp. 1726–1747, 2014.
- [8] N. T. Dantam, Z. K. Kingston, S. Chaudhuri, and L. E. Kavraki, "An Incremental Constraint-Based Framework for Task and Motion Planning," *International Journal of Robotics Research, Special Issue on the 2016 Robotics: Science and Systems Conference*, vol. 37, no. 10, pp. 1134–1151, 2018.
- [9] C. R. Garrett, T. Lozano-Perez, and L. P. Kaelbling, "FFRob: Leveraging symbolic planning for efficient task and motion planning," *The International Journal of Robotics Research*, vol. 37, no. 1, pp. 104–136, 2018.
- [10] A. Thomas, F. Mastrogiovanni, and M. Baglietto, "MPTP: Motion-planning-aware task planning for navigation in belief space," *Robotics and Autonomous Systems*, vol. 141, p. 103786, 2021.
- [11] M. Stilman, J.-U. Schamburek, J. Kuffner, and T. Asfour, "Manipulation planning among movable obstacles," in *Proceedings 2007 IEEE international conference on robotics and automation*, pp. 3327–3332, IEEE, 2007.
- [12] M. Dogar and S. Srinivasa, "A framework for push-grasping in clutter," in *Proceedings of Robotics: Science and Systems VII* (N. R. Hugh Durrant-Whyte and P. Abbeel, eds.), (Los Angeles, CA, USA), MIT Press, June 2011.
- [13] A. Krontiris and K. E. Bekris, "Dealing with Difficult Instances of Object Rearrangement," in *Proceedings of Robotics: Science and Systems XI*, (Rome, Italy), July 2015.
- [14] H. Karami, A. Thomas, and F. Mastrogiovanni, "Task Allocation for Multi-robot Task and Motion Planning: A Case for Object Picking in Cluttered Workspaces," in *AIxIA 2021 – Advances in Artificial Intelligence*, (Cham), pp. 3–17, Springer International Publishing, 2022.
- [15] L. Zhang, Y. J. Kim, and D. Manocha, "Efficient cell labelling and path non-existence computation using c-obstacle query," *The International Journal of Robotics Research*, vol. 27, no. 11–12, pp. 1246–1257, 2008.
- [16] Z. McCarthy, T. Bretl, and S. Hutchinson, "Proving path non-existence using sampling and alpha shapes," in *2012 IEEE international conference on robotics and automation*, pp. 2563–2569, IEEE, 2012.
- [17] S. Li and N. T. Dantam, "Towards general infeasibility proofs in motion planning," in *2020 IEEE/RSJ International Conference on Intelligent Robots and Systems (IROS)*, pp. 6704–6710, IEEE, 2020.
- [18] A. Varava, J. F. Carvalho, D. Kragic, and F. T. Pokorný, "Free space of rigid objects: Caging, path non-existence, and narrow passage detection," *The international journal of robotics research*, vol. 40, no. 10–11, pp. 1049–1067, 2021.
- [19] J. Basch, L. J. Guibas, D. Hsu, and A. T. Nguyen, "Disconnection proofs for motion planning," in *Proceedings 2001 ICRA. IEEE International Conference on Robotics and Automation (ICRA)*, vol. 2, pp. 1765–1772, IEEE, 2001.
- [20] S. Li and N. T. Dantam, "A sampling and learning framework to prove motion planning infeasibility," *The International Journal of Robotics Research*, vol. 0, no. 0, p. 02783649231154674, 2023.
- [21] Y. Sung and P. Stone, "Motion Planning (In)feasibility Detection using a Prior Roadmap via Path and Cut Search," in *Proceedings of Robotics: Science and Systems*, (Daegu, Republic of Korea), July 2023.
- [22] A. M. Wells, N. T. Dantam, A. Shrivastava, and L. E. Kavraki, "Learning feasibility for task and motion planning in tabletop environments," *IEEE robotics and automation letters*, vol. 4, no. 2, pp. 1255–1262, 2019.
- [23] D. Driess, J.-S. Ha, and M. Toussaint, "Learning to solve sequential physical reasoning problems from a scene image," *The International Journal of Robotics Research*, vol. 40, no. 12–14, pp. 1435–1466, 2021.
- [24] K. Hauser, "Minimum constraint displacement motion planning," in *Proceedings of Robotics: Science and Systems IX*, (Berlin, Germany), June 2013.
- [25] A. Thomas and F. Mastrogiovanni, "Minimum Displacement Motion Planning for Movable Obstacles," in *Intelligent Autonomous Systems 17*, (Cham), pp. 155–166, Springer Nature Switzerland, 2023.
- [26] A. Thomas, G. Ferro, F. Mastrogiovanni, and M. Robba, "Computational tradeoff in minimum obstacle displacement planning for robot navigation," in *2023 IEEE International Conference on Robotics and Automation (ICRA)*, pp. 3635–3641, 2023.
- [27] K. Hauser, "The minimum constraint removal problem with three robotics applications," *The International Journal of Robotics Research*, vol. 33, no. 1, pp. 5–17, 2014.
- [28] A. Thomas, F. Mastrogiovanni, and M. Baglietto, "Revisiting the Minimum Constraint Removal Problem in Mobile Robotics," in *Intelligent Autonomous Systems 18*, (Cham), pp. 31–41, Springer Nature Switzerland, 2024.
- [29] C. Mccoid and M. J. Gander, "A provably robust algorithm for triangle-triangle intersections in floating-point arithmetic," *ACM Transactions on Mathematical Software (TOMS)*, vol. 48, no. 2, pp. 1–30, 2022.
- [30] L. E. Kavraki, "Computation of configuration-space obstacles using the fast fourier transform," *IEEE Transactions on Robotics and Automation*, vol. 11, no. 3, pp. 408–413, 1995.
- [31] B. Curto and V. Moreno, "Mathematical formalism for the fast evaluation of the configuration space," in *Proceedings 1997 IEEE International Symposium on Computational Intelligence in Robotics and Automation CIRA'97: Towards New Computational Principles for Robotics and Automation*, pp. 194–199, IEEE, 1997.